analytical chemistry

pubs.acs.org/ac
Article

Accurate Determination of Circulatory Lipids Using a Combination of HILIC-MRM and RPLC-PRM

Kyeong-Seog Kim,[#] Jae-Seung Lee,[#] Seung Seok Han, and Joo-Youn Cho*

Cite This: *Anal. Chem.* 2025, 97, 9713−9721
Read Online

ABSTRACT: Circulatory lipids are important markers for characterizing disease phenotypes; however, accurately determining lipid species remains a significant challenge in lipidomic analysis. Here, we present a novel analytical workflow for accurate lipidome characterization in human plasma using mass spectrometry (MS) through the integration of hydrophilic interaction liquid chromatography (HILIC) and reversed-phase liquid chromatography (RPLC). This workflow enables rapid screening of 1,966 lipid species across 18 lipid classes using HILIC-multiple reaction monitoring (MRM), which enables facile identification of lipid species by lipid class-based separations. In the NIST Standard Reference Material for Human Plasma (SRM 1950), 489 lipid species were identified using HILIC-MRM and subsequently analyzed with RPLC-parallel reaction monitoring (PRM) to resolve potential lipid isobars within the same lipid class. Notably, RPLC-PRM identified 70 additional lipidomic features in SRM 1950 that were not detectable with HILIC-MRM. Furthermore, a high correlation (Pearson correlation coefficient = 0.81) was observed regarding the concentrations of lipid species not carrying isobaric interferences in between HILIC-MRM and RPLC-PRM, indicating that the individual lipid concentrations measured by each platform can be integrated. The workflow was further applied to a cohort of 284 human plasma samples from chronic kidney disease (CKD) patients, successfully profiling lipidomic phenotypes across CKD subtypes. These findings demonstrate that combining HILIC-MRM and RPLC-PRM as complementary platforms enhances the accuracy and comprehensiveness of lipidomic analysis.

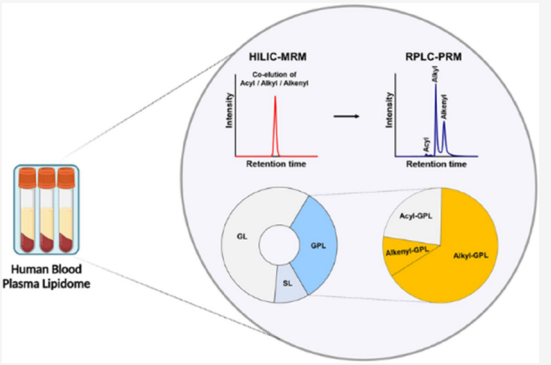

INTRODUCTION

The human blood plasma lipidome provides valuable insights into metabolism and physiology in health and disease.[1] Circulatory lipids serve as crucial markers for diagnosing diseases and monitoring their progression.[2,3] Notably, understanding changes in the circulating lipidome within disease cohorts can reveal potential therapeutic targets.[2,3] However, lipid profiling of circulatory lipids remains challenging due to the vast number and molecular complexity of lipid species present.[4]

Mass spectrometry (MS)-based methodologies have been widely used for lipid characterization at the omics level, leveraging structural properties to investigate the clinical relevance of specific lipid profiles.[5−9] Despite these advancements, identifying isomeric and isobaric lipids remains a significant challenge, as annotation of individual lipid species is often limited.[10,11] To address these limitations, liquid chromatography (LC) has been employed to separate lipid isomers and isobars effectively.[12−14] Among LC-MS-based lipidomic approaches, the most commonly used separation techniques include hydrophilic interaction liquid chromatography (HILIC), normal-phase liquid chromatography (NPLC), and reversed-phase liquid chromatography (RPLC), each with distinct separation mechanisms.[15−19]

HILIC separates lipid classes based on the polarity of their headgroups, leading to the coelution of lipids within the same class.[9] A key advantage of HILIC lies in its enhanced sensitivity in LC-MS due to the high organic content of the eluent, which improves analyte ionization.[20] However, isobars and isomers are present even within the same lipid class.[21,22] The covalent bonds associated with the lipid headgroup—specifically ester (acyl-), ether (1-O-alkyl, denoted as "O"), and vinyl-ether (1-O-alk-1′-enyl, denoted as "P")—generate isomeric and isobaric lipid species within the lipid class, complicating their separation when using a HILIC column.[23] For instance, phosphatidylethanolamine (PE) (O-35:1) (m/z 716.56; $[M-H]^-$ as an adduct type), containing an ether bond, shares the same nominal m/z (mass difference 0.0364 Da) as diacyl PE (34:1) (m/z 716.5236; $[M-H]^-$ as an adduct type). These species coelute because HILIC column separation is based on

Received: November 27, 2024
Revised: April 21, 2025
Accepted: April 25, 2025
Published: May 2, 2025

the polar headgroup.[21,22] In contrast, an RPLC column separates lipid species by the hydrophobicity of their fatty acid or alkyl chains.[9] Due to this chemical property, the RPLC system provides enhanced separation, enabling high-level identification of isomeric and isobaric compounds within the same lipid class.[15] Thus, RPLC-MS/MS and HILIC-MS/MS exhibit distinct advantages based on their respective chemical properties, highlighting their complementary roles in lipidomics methodologies.[24−26]

Targeted lipidomics using LC-MS/MS have driven significant advancements in analytical development. Specifically, the application of collision-induced dissociation and MS analysis has facilitated the identification of fatty acyl chain lipid species.[23] In targeted lipidomic analysis, multiple reaction monitoring (MRM) with triple quadrupole-MS is widely employed[27−30] due to its ability to monitor the mass transition from precursor ions to product ions with enhanced sensitivity. However, the accuracy of lipid species identification is constrained by the low mass resolution (isolation window of 0.7 Da) of the quadrupole mass filter.[27,31] To address this limitation, high-resolution MRM, also known as parallel reaction monitoring (PRM), serves as a complementary technique by monitoring fragmented ions with high-resolution MS analyzers, such as time-of-flight or Fourier transform instruments.[15] Despite its advantages, PRM suffers from a relatively slow scan speed compared to the MRM method.[27,32]

Here, we propose an advanced analytical strategy combining HILIC-MRM with RPLC-PRM for comprehensive lipidome analysis in human plasma. In this workflow, the circulatory lipidome is initially analyzed using HILIC-MRM, which enables rapid and facile measurement of lipid species through lipid class-based separation. Subsequently, RPLC-PRM is employed to identify potential lipid isobars within the same lipid class that could not be resolved by the HILIC-MRM system. This developed workflow was applied to a large cohort of 284 human plasma samples to characterize the circulatory lipid profiles of four subtypes of chronic kidney disease (CKD). Notably, CKD was associated with dyslipidemia, characterized by elevated levels of neutral lipids like triacylglycerides.[33−36] However, the specific lipid profiles linked to each CKD subtype remained unclear. Our objective was to demonstrate that this platform offers a reliable and reproducible omics-level workflow capable of determining distinct lipid profiles across CKD subtypes.

EXPERIMENTAL SECTION

Sample Collection. The human plasma samples from the CKD cohort (n = 284) comprising healthy controls (n = 66) and four CKD subtypes, including diabetic nephropathy (DN, n = 64), hypertensive nephropathy (HN, n = 24), immunoglobulin A nephropathy (IgAN, n = 66), and membranous nephropathy (MN, n = 64) were collected at Seoul National University Hospital under the approval of the institutional review board (IRB) of the Seoul National University College of Medicine (IRB number: H-2104-120-1214). Detailed diagnostic criteria for the CKD cohort and procedures for plasma sample collection are provided in the Supporting Information.

The mouse study for the exploration of endogenous lipids to the other matrix e.i., serum and liver tissue was obtained from the SMC Laboratories (SMC Laboratories Inc., Tokyo, Japan). Mouse experiment and sample preparation protocol for lipidomics analysis is described in Supporting Information.

Chemicals and Reagents. Chemicals and reagents are described in Supporting Information.

Preparation of Internal Standard Mixture. Deuterated lipids were used as internal standards (IS) for normalization and quantification in this study. Briefly, 18 deuterated lipids were mixed in methyl-*tert* butyl ether, and all the samples were spiked with the IS mixture at the target concentrations outlined in Table S1.

Sample Preparation. Human plasma samples, including those from the CKD cohort and SRM 1950, were thawed on ice prior to lipid extraction. For extraction, 400 μL of 80% isopropanol (IPA) was added to 50 μL of each sample. The mixtures were vortexed and centrifuged for 5 min at 18,341 × g and 4 °C. Subsequently, 200 μL of the supernatant was transferred into two Eppendorf SafeLock tubes and dried under N_2 gas. The dried pellets were reconstituted with either 100 μL of 95% acetonitrile (ACN) containing 10 mM ammonium acetate (AmAc) for HILIC-MRM analysis or 200 μL of ACN:Water:IPA (40:24:36) containing 10 mM AmAc for RPLC-PRM analysis.

LC-MS Analysis. HILIC-MRM analysis was performed using an ACQUITY UPLC I-Class PLUS System coupled with a SCIEX Triple Quad 5500 Mass Spectrometer (Waters, Milford, MA, USA) operated in positive and negative ionization modes. Chromatographic separation was achieved on an ACQUITY Premier BEH Amide column (1.7 μm, 100 × 2.1 mm I.D., Waters, Milford, MA, USA) using mobile phases A (ACN:Water = 95:5) and B (ACN:Water = 50:50), both containing 10 mM AmAc. The injector needle was washed with ACN:Water (95:5) after each injection, and the injection volume was set to 2 μL. The gradient elution program was as follows: the system was initially maintained at 0.1% B for 2 min, followed by an increase to 80% B over 3 min. The gradient was returned to the initial condition (0.1% B) within 0.1 min and equilibrated for 3 min at the starting condition. The flow rate was set to 300 μL/min, the column temperature was maintained at 40 °C, and the sample injection volume was 2 μL. Optimized ion source parameters included a voltage of 5500 V in positive mode and −4500 V in negative mode, an ion source temperature of 400 °C, and GS1 and GS2 settings of 30 and 35 psi, respectively. Curtain gas and collision-activated dissociation gas pressures were maintained at 20 and 6 psi. A scheduled MRM (sMRM) algorithm with a retention time (t_R) window of 1 min was applied. Specific sMRM parameters are detailed in Table S2.

The method for accurate determination of isomeric and isobaric lipid species was implemented using an RPLC-PRM setup. Analyses were conducted on a Vanquish UHPLC system coupled with an Orbitrap Exploris 120 (Thermo Scientific, San Jose, CA, USA). Chromatographic separation was achieved using an ACQUITY UPLC HSS T3 column (1.8 μm, 100 × 2.1 mm I.D., Waters, Milford, MA, USA) with a mobile phase A comprising ACN:Water of 60:40 and phase B comprising ACN:IPA of 10:90, both containing 10 mM AmAc. A linear gradient elution was applied, beginning at 40% B for 1 min, increasing from 40 to 65% B over 4 min, from 65 to 95% B over 5 min, held at 95% B for 2 min, followed by a rapid return to 40% B over 0.1 min, and re-equilibration at 40% B for 6 min. The flow rate, column temperature, and injection volume were set at 250 μL/min, 50 °C, and 10 μL, respectively. Ion source parameters were configured with a voltage of −4500 V in negative mode, sheath gas at 60 Arb, auxiliary gas at 15 Arb, sweep gas at 1 Arb, and an ion transfer tube temperature of

https://doi.org/10.1021/acs.analchem.4c06409
Anal. Chem. 2025, 97, 9713−9721

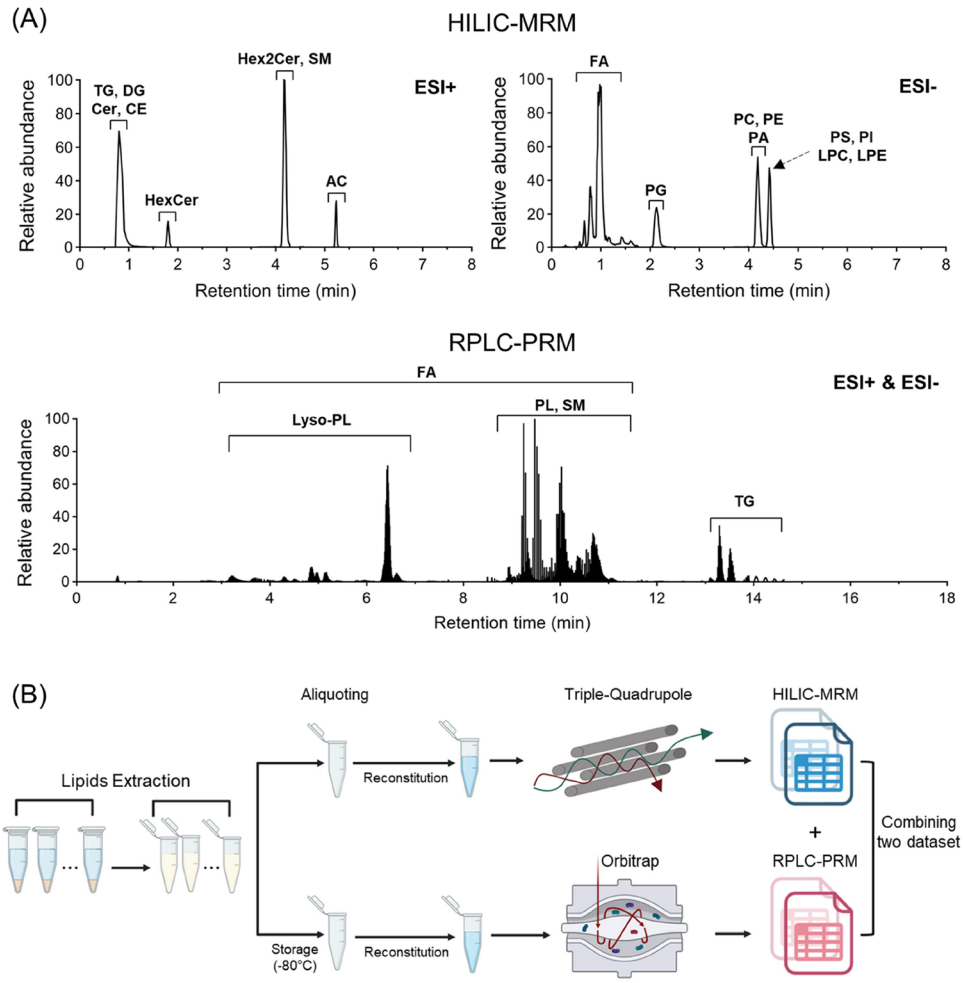

Figure 1. Schematic workflow combining HILIC-MRM and RPLC-PRM analyses. (A) HILIC separates lipids based on the polarity of their headgroups, while RPLC separates lipids according to the hydrophobicity of their fatty acyl chains, considering the polarity of the lipid headgroup. (B) To integrate data sets from HILIC-MRM and RPLC-PRM, human plasma samples were aliquoted after lipid extraction. Lipids were first analyzed using HILIC-MRM, followed by RPLC-PRM, enabling accurate identification of isomeric and isobaric lipids (image created by Biorender). PL, phospholipid.

380 °C. The vaporizer temperature was maintained at 350 °C. Full MS scan data were acquired over an m/z range of 67−1000 in dual-polarity mode at a resolution of 120,000 FWHM at m/z 200, while product ion scans were obtained over the same m/z range at a resolution of 15,000 FWHM at m/z 200. Both MS scan and product ion scan data were acquired in centroid mode. Transition parameters for identifying isomeric and isobaric lipids are detailed in Table S3.

Lipid Identification. Identification of lipids using HILIC-MRM was accomplished by determining the t_R of lipid class-specific IS. The nomenclature and structural levels of lipid annotation adhered to the recent LIPID MAPS update.[6] Specifically, MS/MS transitions for lipid annotation included head groups and fatty acyl chains for glycerolipids (GLs), long-chain bases for sphingolipids (SPs), and fatty acyl-based transitions for glycerophospholipids (GPs) (Figure S1).[37,38]

For lipid identification in RPLC-PRM data, MS/MS fragmentation patterns obtained through product ion scan mode were utilized. Raw data from product ion scan mode were manually examined using Freestyle software (Thermo Scientific). Lipid annotation for the accurate determination of isobaric and isomeric lipids was based on previously reported studies.[39−44] Detailed identification criteria are provided in the Supporting Information, with the identified lipid species summarized in Table S4.

Method Validation. The method validation process including limit of quantification (LOQ), linearity range, interday precision, standard addition approach, matrix effect, and recovery was performed by referring to the relevant bioanalytical guidelines[45,46] and previous studies.[8,9,47−49] Detailed validation procedures are described in Supporting Information.

Data Analysis. Peak area integration for HILIC-MRM analysis was performed using Analyst version 1.6.3 (AB SCIEX), while RPLC-PRM data were processed using Skyline version 24.1 with the small molecule target function.[6,50] For lipid quantification in both HILIC-MRM and RPLC-PRM analyses, concentrations were calculated using the isotope dilution approach. Specifically, the peak area of each lipid was normalized by dividing it by the peak area of the corresponding deuterated IS in the same lipid class, as described previously.[51] The resulting value was then multiplied by the amount of IS added to calculate the lipid concentration.[9] In HILIC-MRM data, the overall contribution of heavy isotopes to MRM transition intensities was dependent on their molecular position in the fragmentation pattern.[38] Corrections for

https://doi.org/10.1021/acs.analchem.4c06409
Anal. Chem. 2025, 97, 9713−9721

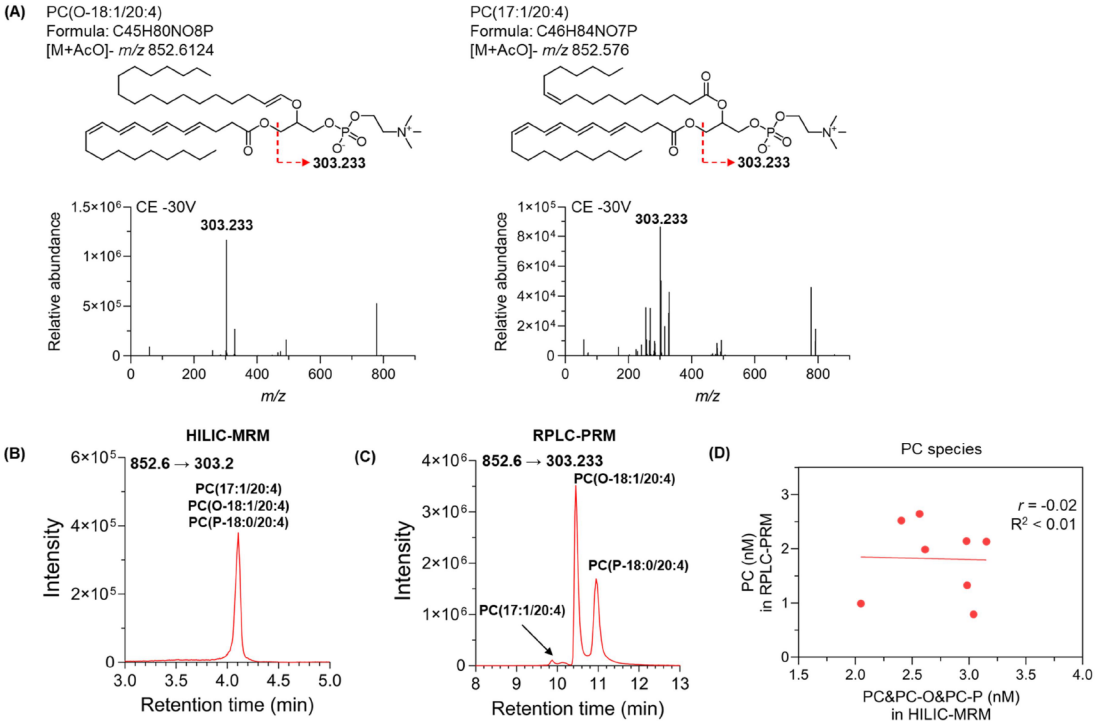

Figure 2. (A) Chemical structures, adduct types, fragmentation patterns, and MS/MS spectrum of two lipid isobars, PC (17:1/20:4) and PC (O-18:1/20:4). (B and C) Chromatograms of lipids analyzed using (B) HILIC column and (C) RPLC column, both with the same MRM transition, from pooled CKD plasma samples. (D) Comparison of concentrations of eight PC species analyzed by HILIC (*X*-axis) and RPLC (*Y*-axis). Pearson correlation analysis and linear regression were used for comparison; detailed parameters and concentrations are provided in Table S5. *r*, Pearson correlation coefficient; R^2, coefficient of determination.

isotopic overlap during lipid class-based chromatographic separation were made using the Shiny app of LICAR, developed by SLING.[38] Detailed descriptions of strategy for integration of HILIC-MRM and RPLC-PRM lipidomic data and the statistical analysis are provided in the Experimental Section of Supporting Information and Scheme S1.

RESULTS AND DISCUSSION

Concept of Lipidome Measurement Strategy Using a Combination of HILIC and RPLC. The human plasma lipidome comprises thousands of lipid species, including numerous isomeric and isobaric lipids within the same lipid class, which are challenging to profile using conventional methods. To accurately characterize these complex lipids, we developed an analytical strategy combining HILIC-MRM and RPLC-PRM data sets. Figure 1 illustrates the workflow for the accurate identification of the plasma lipidome using a targeted lipidomic analysis approach. In Figure 1A, lipid separation is shown using both HILIC and RPLC columns. The HILIC column separates lipids based on their headgroup polarity, enabling the rapid and efficient identification of lipid species, while the RPLC column separates lipids according to the hydrophobicity of their fatty acyl chains in conjunction with the polarity of the lipid headgroup. This dual approach allows for the differentiation of isomeric and isobaric lipid species. The integrated strategy combining HILIC-MRM and RPLC-PRM data is depicted in Figure 1B. Lipids extracted from human plasma were divided into two equal aliquots and analyzed sequentially. HILIC-MRM measured thousands of lipid species in the first step, followed by RPLC-PRM to identify potential isobaric and isomeric lipids. RPLC-PRM was then employed for the accurate quantification of lipid isobars. High-resolution MS/MS instrumentation in the RPLC analysis was critical to this approach, as PRM allowed accurate lipid identification while minimizing interference from other lipid species. For example, when identifying PC (16:0/18:1) at t_R 10.4 min in the RPLC column, unit-resolution MRM (mass accuracy <0.6 Da) detected overlapping isotopes ([M + 2]) from PC (16:0/18:2) at t_R 10.1 min. In contrast, high-resolution PRM (mass accuracy <5 ppm) accurately identified PC (16:0/18:1) (Figure S2). Given the limited availability of lipid standards, PRM transitions proved more reliable than MRM transitions for the accurate identification of target lipids.

The advantage of using RPLC-PRM as a complementary platform to HILIC-MRM for the identification of lipid isobars is demonstrated in Figure 2. The analysis focused on the separation of PC and ether PC, which coelute in HILIC-MRM. For example, PC (O-18:1/20:4) and PC (17:1/20:4) are isobars with precursor ions at *m/z* 852.6124 and *m/z* 852.576, respectively, and $[M + AcO]^-$ as the adduct type (Figure 2A). These isobaric lipids share a common fragmentation ion, *m/z* 303.233 ($[FA20:4 - H]^-$), in the MS/MS spectrum, which is typically used as the product ion in MRM transitions for identifying lipid species at the fatty acyl chain level. In the HILIC method, transitions (852.6 > 303.2) produced a single coeluting peak encompassing PC (17:1/20:4), PC (O-18:1/20:4), and PC (P-18:0/20:4) (Figure 2B). Conversely, RPLC-PRM transitions (852.6 > 303.233) successfully separated these lipids, distinguishing PC (17:1/20:4), PC (O-18:1/20:4), and PC (P-18:0/20:4) based on their respective t_R of 9.5, 10.3, and 11.1 min (Figure 2C). Notably, RPLC-PRM identified PC (P-18:0/20:4) as an isomer of PC (O-18:1/20:4). To evaluate whether the interference of isobaric lipids, including PC-O and PC-P, affects the accuracy of PC species

https://doi.org/10.1021/acs.analchem.4c06409
Anal. Chem. 2025, 97, 9713−9721

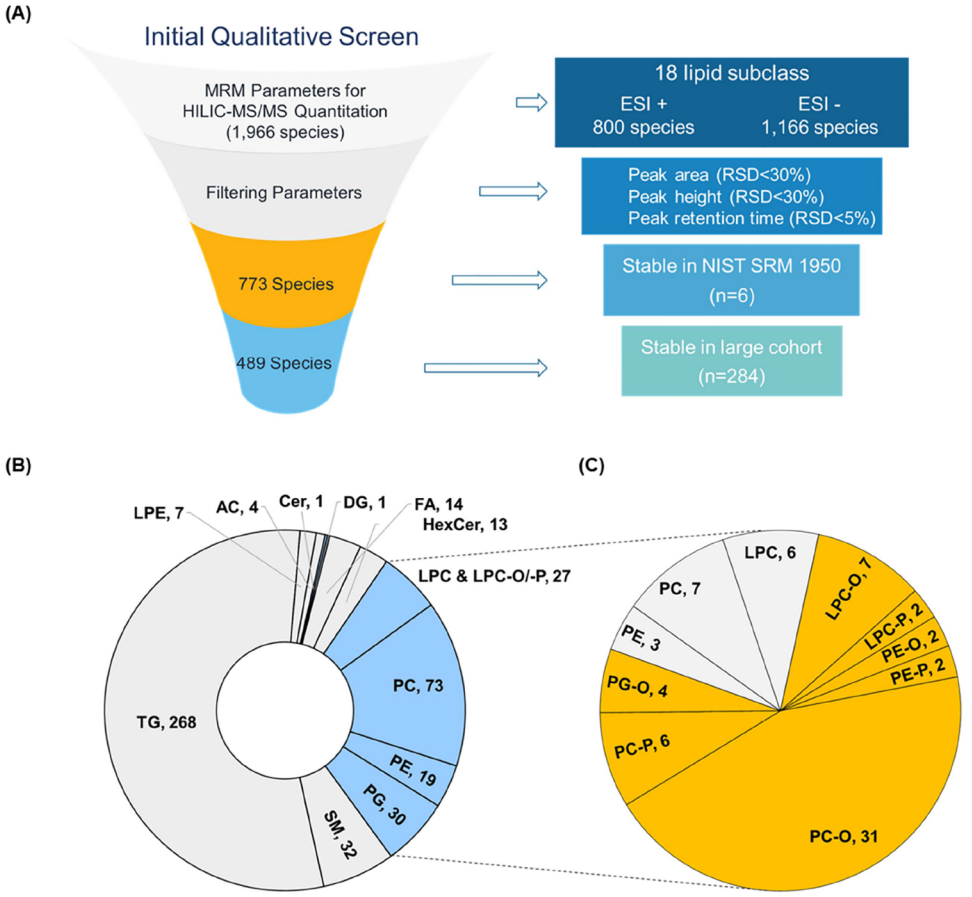

Figure 3. Analytical workflow for human plasma samples, progressing from initial qualitative screening to reliable quantification. (A) Initial qualitative screening of SRM 1950 plasma identified 800 lipid species in ESI (+) mode and 1,166 species in ESI (−) mode (Table S2). Among these, 773 stable lipids were confirmed in SRM 1950 (n = 6), and 489 lipid species were further quantified during the CKD cohort analysis (n = 284). (B) Pie chart displaying the lipid species distribution by class in SRM 1950, as analyzed using the HILIC-MRM. (C) Lipid species detected via HILIC-MRM were subsequently analyzed using RPLC-PRM, revealing an additional 70 isobaric and isomeric lipids.

measurement using HILIC-MRM, eight PC species were analyzed via both HILIC-MRM and RPLC-PRM (Figure 2D and Table S5). Due to the coelution of isobaric lipids, the concentrations of PC measured by HILIC-MRM were consistently higher than those measured by RPLC-PRM, resulting in a low correlation coefficient (r = −0.02). These findings demonstrate that lipid assay using HILIC column is prone to interference from coeluting isobaric lipids. Incorporating a separation system like RPLC column enables the resolution of such isobars, ensuring more accurate lipid quantification.

Identification of Isobaric and Isomeric Lipids Using RPLC-MS/MS. We next applied the combined HILIC-MRM and RPLC-PRM workflow to human plasma. First, we measured the LOQ levels and linearity ranges of the spiked IS mixture from SRM 1950 in both analytical platforms (Table S6). Among the 18 target lipid classes, 16 exhibited lower LOQ levels in both platforms—except for DG and CE—compared to other MS techniques, such as ion mobility-MS and direct infusion (DI)-MRM.[52,53] Lipid classes, including AC, HexCer, SM, FA, LPC, LPE, PC, PE, and PG, had similar LOQ levels between platforms (difference ≤ 2.0-fold). However, higher LOQ levels were observed in the HILIC-MRM platform compared to the RPLC-PRM platform for DG (4-fold), Hex2Cer (4-fold), PA (16-fold), PI (64-fold), and PS (8-fold), whereas TG (4-fold), Cer (130-fold), and DhCer (32-fold) exhibited higher LOQ levels in RPLC-PRM. CE was not detected in RPLC-PRM within the concentration ranges of 8.1−425,761 nM. Using HILIC-MRM, 1966 lipid species were initially screened, and 773 lipid species were detected in SRM 1950 across six replicates (Table S7). Among these, 489 lipid species with RSDs below 30% across SRM 1950 (n = 12) were identified during the analysis of a large cohort (n = 284) (Figure 3A,B). The precursor ions and corresponding collision energies for these 489 lipid species were subsequently analyzed in product ion mode (m/z range: 67−1000) using RPLC-MS/MS, identifying an additional 70 lipids in SRM 1950 (Figure 3C). For lipid identification in RPLC-MS/MS, both the exact masses of precursor ions in MS scan mode and the fragmented ions in MS/MS product ion mode were utilized (Figure S3). The major lipid classes identified through RPLC-MS/MS included ether lipids such as PC-O, PC-P, PE-O, PE-P, PG-O, LPC-O, and LPC-P, which exhibited similar LOQ levels across both platforms. The 22 overlapping lipids from HILIC-MRM that affected by the isobaric and isomeric interferences were excluded (workflow for integration of two data sets is described in Experimental Section of Supporting Information and Scheme S1). To evaluate the reproducibility of the integrated lipid data set, interday precision was measured for 537 lipid species (467 species from HILIC-MRM and 70 species from RPLC-PRM) across different batches (Table S8). Highly reproducible results were obtained, with 88% of lipid

https://doi.org/10.1021/acs.analchem.4c06409
Anal. Chem. 2025, 97, 9713−9721

species exhibiting RSDs below 20% and 95% below 30% (Figure S4). These results are consistent with a previous HILIC-MRM study, which demonstrated that 85% of total lipid species (RSD < 20%) remained stable in interday precision measurements from SRM 1950.[5]

We applied the method to other biological matrices, including liver and serum samples obtained from five mice, enabling the detection of 663 lipid species (544 from HILIC-MRM and 119 from RPLC-PRM) in liver and 473 lipid species (383 from HILIC-MRM and 90 from RPLC-PRM) in serum (Figure S5, Tables S9 and S10). Further, we evaluated the matrix effect and recovery in these biological matrices by comparing the peak areas of the IS mixture (Table S11). Matrix effect evaluation across five biological origins (three replicates per origin) per matrix yielded reliable results, with 90% of the 108 lipid standards exhibiting matrix effects of less than 20%. Recovery measurements also demonstrated a consistent extraction efficiency, with 88% of lipid species showing RSDs below 20% (n = 3), though mean recovery values varied depending on the biological matrix. Interestingly, extraction recovery differed by analytical platform, even for the same lipid class. For instance, recoveries of PE (15:0/18:1-d_7) from SRM 1950 were 29.3% in HILIC-MRM and 80.4% in RPLC-PRM. This discrepancy is likely due to severe matrix suppression in HILIC separation, highlighting the necessity of correcting lipid signals using matrix-matched IS signals for accurate quantification across diverse biological matrices, as previously described.[54−56]

Concordance of Lipid Concentrations Measured with HILIC-MRM and RPLC-PRM. We aimed to integrate the lipid concentrations measured by HILIC-MRM and RPLC-PRM while minimizing isobaric and isomeric interferences. For successful integration, the concentrations obtained from both platforms needed to be concordant. To assess this, we compared lipid concentrations between HILIC-MRM and RPLC-PRM using the standard addition approach. The concentration of PC (16:0/18:2) was consistent between two methods, calculated as 11.7 μM with HILIC-MRM and 11.3 μM with RPLC-PRM, corresponding to a relative error of 3.5% (Figure 4A). Additionally, lipid species with isobaric interferences were compared (Figure 4B and Table S12). The concentrations of 201 lipids exhibited a strong correlation (r = 0.81 and R^2 = 0.65). Furthermore, we compared the correlation between the integrated lipidomic data collected from HILIC-MRM and RPLC-PRM and the previously reported RPLC-MRM lipidomic data from Huynh et al.[41] A high correlation was observed (r = 0.85, R^2 = 0.73) between the two data sets (Figure S6 and Table S13). These results indicate that the concentrations of individual lipid species measured by HILIC-MRM and RPLC-PRM were highly concordant, thereby supporting the integration of the two lipidomic data sets.

Characterization of Circulatory Lipid Biomarkers in the CKD Cohort. As a proof of concept, we evaluated circulatory lipid biomarkers in four CKD subtypes classified by kidney biopsy. Using our analytical workflow, we identified 145 lipids that significantly altered as determined by ANOVA and characterized unique lipidomic patterns in patients with different CKD subtypes (adjusted p-value <0.05; Figure 5 and Table S14). Among these, 26 lipid species comprising 1 AC, 16 GPs, and 9 SPs—were associated with CKD progression and linked to the four CKD subtypes (Figure 5B,C). For instance, the AC (2:0) concentrations were

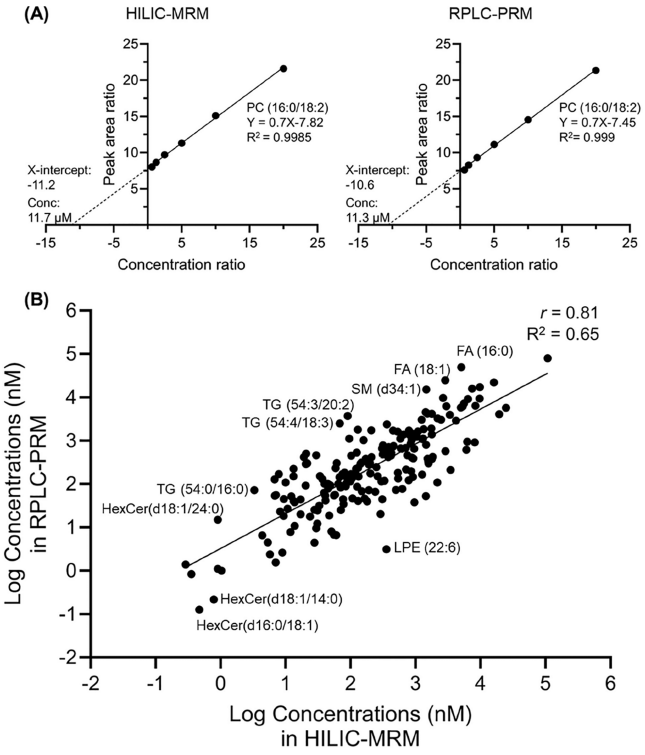

Figure 4. Concordance of lipid concentrations measured using HILIC-MRM and RPLC-PRM. (A) Standard addition method for quantifying PC (16:0/18:2) in SRM 1950 plasma using HILIC-MRM and RPLC-PRM. (B) Comparison of lipid species without isobaric interference. Black circles represent the mean concentrations of lipid species (n = 6 for SRM 1950) measured using HILIC-MRM (X-axis) and RPLC-PRM (Y-axis). r, Pearson correlation coefficient; R^2, coefficient of determination.

elevated in all CKD subtypes compared to healthy subjects, supporting previous observations that serum AC (2:0) levels rise as renal function declines in CKD patients.[57] This finding demonstrates that lipidomic profiles can effectively differentiate CKD patients from healthy individuals.

Figure 5D presents CKD subtype-specific lipidomic profiles. We observed elevated TG levels in the DN group, whereas no significant increase was noted in other CKD subtypes, consistent with previous studies on the mechanisms of dyslipidemia.[58,59] Additionally, ether PCs, such as PC (O-17:1/20:3), PC (O-17:1/20:4), and PC (P-20:1/20:4), were downregulated in the HN group compared to the HC. Given that hypertension is known to alter the plasma lipidome by reducing ether lipid content,[60] this result suggests that ether PC alterations may contribute to HN pathophysiology. Furthermore, SP metabolism is closely related to immune homeostasis in the context of inflammation,[61] aligning with recent findings of decreased SMs in patients with IgAN.[62] MN subtype also displayed distinct lipidomic profiles, including elevated levels of three ether PCs and SM (d33:1) (Figure 5D). Previous studies have reported that ether lipids and sphingolipids are metabolically coregulated in cellular response,[63] underscoring their importance in maintaining cellular homeostasis. Finally, we assessed the diagnostic performance of lipidomic features in classifying CKD subtypes. Cohen's effect size was calculated for the lipid species described in Figure 5D to quantify the magnitude of the differences between groups (Cohen's effect size $|d| \geq 0.5$).

https://doi.org/10.1021/acs.analchem.4c06409
Anal. Chem. 2025, 97, 9713−9721

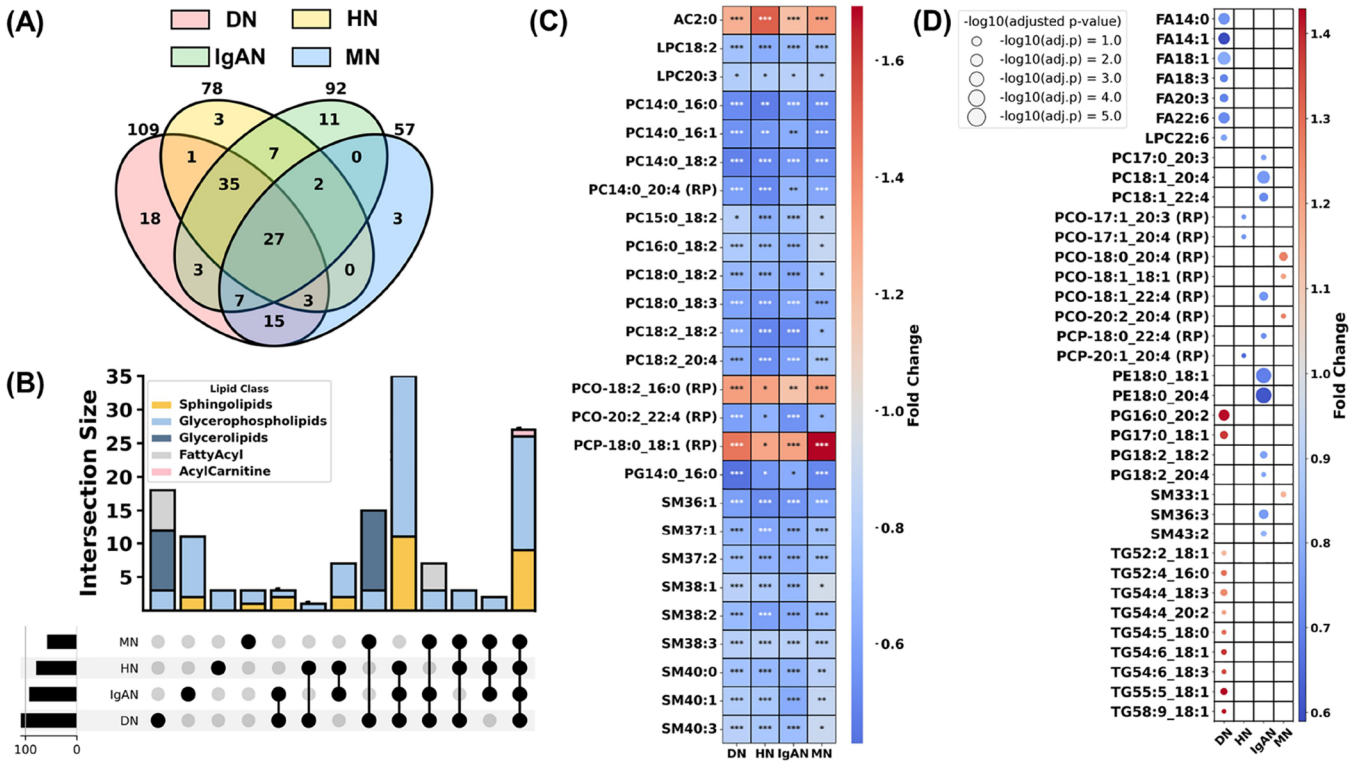

Figure 5. Characterization of subtype-specific circulatory lipid profiles in the CKD cohort. (A) Venn diagram depicting distinct differential lipids, overlapping lipids, and common differential lipids across CKD subtypes (adjusted *p*-value <0.05). (B) UpSet plot illustrating distinct lipid distributions across CKD subtypes, with stacked bars representing the proportion of shared and unique differential lipid classes for each subtype. (C) Heatmap showing the median fold change of lipids that exhibit significant that exhibit all CKD subtypes compared to the HC group. $^{*}P < 0.05$; $^{**}P < 0.01$; $^{***}P < 001$. (D) Bubble plot highlighting lipidomic profiles specifically altered in each CKD subtype. RP denotes lipid species identified using RPLC-PRM.

Based on this analysis, 15, 3, 10, and 3 lipids were selected for the development of classification models for DN, HN, IgAN, and MN, respectively (Figure S7 and Table S15). Machine learning-based analyses, including Random Forest, Support Vector Machine, and K-Nearest Neighbors, demonstrated reliable classification performance across all three models (AUROC > 0.7; Figure S8).[64] Collectively, our findings highlight circulating lipids as potential diagnostic targets for CKD subtyping.

CONCLUSIONS

This study described the lipidomics workflow that integrates HILIC-MRM and RPLC-PRM. The HILIC column separates lipids based on their lipid headgroup, facilitating identification. However, some lipid species exhibited overlapping t_R and MS/MS transitions, potentially leading to significant identification errors. To address this, we demonstrated how the RPLC-PRM platform complements HILIC-MRM by resolving whether lipid species detected via HILIC-MRM contain isobaric or isomeric lipids. It is well-established that even-chain lipids are more abundant than odd-chain lipids in humans. Previous studies using DI-, NPLC-, or HILIC-MS/MS have annotated lipid signals primarily as even-chain lipids.[5,65] For instance, PC (O-38:5) and PC (37:5) are isobaric lipids with a mass difference of 0.0364 Da, commonly annotated as PC (O-38:5).[65] Additionally, the relative abundance of even- and odd-chain lipids may vary across species. Odd-chain lipids, often produced by bacteria, have been identified in human plasma, likely originating from commensal bacteria or dietary intake.[66,67] These coeluting lipids were effectively separated via sequential analysis using RPLC-PRM. RPLC-PRM provided high selectivity in lipid detection; however, its limited scan speed made it impractical for analyzing several hundred transitions in an 18 min run. In contrast, previous investigations using RPLC-MRM successfully characterized lipidomes on a single platform with a comparatively faster scan rate.[41,68] However, unit-resolution MS in RPLC-MRM may lead to peak selectivity issues due to interference from heavy isotopes of different lipid species.[69] Two-dimensional LC-MS improves lipid selectivity,[70] but generally requires a longer run time for the second LC separation compared to single LC methods.[71,72] To enhance lipid coverage, we integrated HILIC-MRM and RPLC-PRM, enabling the reliable identification of a large number of lipid species across hundreds of research samples while effectively resolving such interferences. This approach outperforms previous methodologies. Furthermore, lipid species detected using HILIC-MRM and RPLC-PRM exhibited a strong correlation in concentration measurements and concordance with values reported in prior studies.[41] Interestingly, numerous studies have shown high correlations between lipid concentrations, regardless of the MS platform used,[5,8] confirming that merging data sets from HILIC-MRM and RPLC-PRM is feasible for quantitative lipid analysis of lipids and enhances the reliability and comprehensiveness of lipid profiling.

Using this advanced workflow, we characterized lipid biomarkers across four CKD subtypes: MN, DN, IgAN, and HN. Lipid markers varied by CKD subtype, revealing distinct lipid class-specific signatures. These findings demonstrate that

https://doi.org/10.1021/acs.analchem.4c06409
Anal. Chem. 2025, 97, 9713−9721

the proposed workflow enables the exploration of diverse biomarkers with extensive lipidomic coverage.

■ ASSOCIATED CONTENT

Supporting Information

The Supporting Information is available free of charge at https://pubs.acs.org/doi/10.1021/acs.analchem.4c06409.

Study design and participants, mouse experiments, lipid nomenclature, chemicals and reagents, criteria for identification of lipid species with RPLC-MS/MS, method validation procedures, data analysis, strategy for integration of HILIC-MRM and RPLC-PRM lipidomic data set, representative MS/MS transitions for each lipid class in this study, comparison of lipid identification using unit-resolution and high-resolution MS/MS analysis, identification of lipids in SRM 1950 using RPLC-MS/MS, interday precision results, pie chart displaying liver and serum lipidome, comparison of lipid concentrations, Cohen's d effect size analysis, ML-based classification (PDF)

Information of deuterated lipid standard, MRM transition parameters for HILIC-MS/MS analysis, product ion scan lists for RPLC-MS/MS analysis, RPLC-PRM transition lists, comparison of concentrations of PC in HILIC-MRM and RPLC-PRM, LOQ and linearities, stable lipids in HILIC-MRM, interday precision results, liver lipidome, serum lipidome, matrix effect and recovery results, lipid concentrations measured in HILIC-MRM and RPLC-MRM, lipid correlation reported by Huynh et al., ANOVA results, and marker lists (XLSX)

■ AUTHOR INFORMATION

Corresponding Author

Joo-Youn Cho − *Department of Biomedical Sciences, Seoul National University College of Medicine, Seoul 03080, Republic of Korea; Department of Clinical Pharmacology and Therapeutics, Seoul National University College of Medicine and Hospital, Seoul 03080, Republic of Korea; Seoul National University, Seoul 08826, Republic of Korea; Kidney Research Institute, Seoul National University Medical Research Center, Seoul 03080, Republic of Korea*; Email: joocho@snu.ac.kr

Authors

Kyeong-Seog Kim − *Department of Biomedical Sciences, Seoul National University College of Medicine, Seoul 03080, Republic of Korea; Department of Clinical Pharmacology and Therapeutics, Seoul National University College of Medicine and Hospital, Seoul 03080, Republic of Korea; Seoul National University, Seoul 08826, Republic of Korea*; orcid.org/0000-0003-3704-1204

Jae-Seung Lee − *Department of Biomedical Sciences, Seoul National University College of Medicine, Seoul 03080, Republic of Korea; Department of Clinical Pharmacology and Therapeutics, Seoul National University College of Medicine and Hospital, Seoul 03080, Republic of Korea; Seoul National University, Seoul 08826, Republic of Korea*; orcid.org/0009-0003-4743-6258

Seung Seok Han − *Department of Internal Medicine, Seoul National University College of Medicine, Seoul 03080, Republic of Korea*

Complete contact information is available at: https://pubs.acs.org/10.1021/acs.analchem.4c06409

Author Contributions

#K.-S.K. and J.-S.L. contributed equally to this work.

Notes

The authors declare no competing financial interest.

■ ACKNOWLEDGMENTS

This work was supported by the National Research Foundation of Korea (NRF) grant funded by the Korea government (MSIT) (RS-2022-NR070165 and RS-2021-NR056442) and supported by the National Institute of Health Research Project (project no. 2021-0317C93-00). The human biospecimens were provided by the Biobank of Seoul National University Hospital, a member of the Korea Biobank Network (KBN4_A03), which is supported by the Korea Centers for Disease Control and Prevention (#4845-303). K.-S.K. and J.-S.L. received a scholarship from the BK21 FOUR education program.

■ REFERENCES

(1) Burla, B.; Arita, M.; Arita, M.; Bendt, A. K.; Cazenave-Gassiot, A.; Dennis, E. A.; Ekroos, K.; Han, X.; Ikeda, K.; Liebisch, G.; Lin, M. K.; Loh, T. P.; Meikle, P. J.; Oresic, M.; Quehenberger, O.; Shevchenko, A.; Torta, F.; Wakelam, M. J. O.; Wheelock, C. E.; Wenk, M. R. *J. Lipid Res.* **2018**, *59* (10), 2001−2017.

(2) Quehenberger, O.; Dennis, E. A. *N. Engl. J. Med.* **2011**, *365* (19), 1812−1823.

(3) Vvedenskaya, O.; Wang, Y.; Ackerman, J. M.; Knittelfelder, O.; Shevchenko, A. *TrAC, Trends Anal. Chem.* **2019**, *120*, 115277.

(4) Quehenberger, O.; et al. *J. Lipid Res.* **2010**, *51* (11), 3299−3305.

(5) Medina, J.; Borreggine, R.; Teav, T.; Gao, L.; Ji, S.; Carrard, J.; Jones, C.; Blomberg, N.; Jech, M.; Atkins, A.; Martins, C.; Schmidt-Trucksass, A.; Giera, M.; Cazenave-Gassiot, A.; Gallart-Ayala, H.; Ivanisevic, J. *Anal. Chem.* **2023**, *95* (6), 3168−3179.

(6) Conroy, M. J.; Andrews, R. M.; Andrews, S.; Cockayne, L.; Dennis, E. A.; Fahy, E.; Gaud, C.; Griffiths, W. J.; Jukes, G.; Kolchin, M.; Mendivelso, K.; Lopez-Clavijo, A. F.; Ready, C.; Subramaniam, S.; O'Donnell, V. B. *Nucleic Acids Res.* **2024**, *52* (D1), D1677−D1682.

(7) Su, B.; Bettcher, L. F.; Hsieh, W. Y.; Hornburg, D.; Pearson, M. J.; Blomberg, N.; Giera, M.; Snyder, M. P.; Raftery, D.; Bensinger, S. J.; Williams, K. J. *J. Am. Soc. Mass. Spectrom.* **2021**, *32* (11), 2655−2663.

(8) Zhang, Z.; Singh, M.; Kindt, A.; Wegrzyn, A. B.; Pearson, M. J.; Ali, A.; Harms, A. C.; Baker, P.; Hankemeier, T. *J. Chromatogr. A* **2023**, *1708*, No. 464342.

(9) Munjoma, N.; Isaac, G.; Muazzam, A.; Cexus, O.; Azhar, F.; Pandha, H.; Whetton, A. D.; Townsend, P. A.; Wilson, I. D.; Gethings, L. A.; Plumb, R. S. *J. Proteome Res.* **2022**, *21* (11), 2596−2608.

(10) Kirkwood, K. I.; Pratt, B. S.; Shulman, N.; Tamura, K.; MacCoss, M. J.; MacLean, B. X.; Baker, E. S. *Nat. Protoc.* **2022**, *17* (11), 2415−2430.

(11) Rustam, Y. H.; Reid, G. E. *Anal. Chem.* **2018**, *90* (1), 374−397.

(12) Cajka, T.; Fiehn, O. *TrAC, Trends Anal. Chem.* **2014**, *61*, 192−206.

(13) Astarita, G.; Ahmed, F.; Piomelli, D. *Methods Mol. Biol.* **2009**, *579*, 201−219.

(14) Holcapek, M.; Liebisch, G.; Ekroos, K. *Anal. Chem.* **2018**, *90* (7), 4249−4257.

(15) Lange, M.; Fedorova, M. *Anal. Bioanal. Chem.* **2020**, *412* (15), 3573−3584.

(16) Zhou, G.; Lu, J.; Xu, T.; Lu, Y.; Chen, W.; Wang, J.; Ke, M.; Shen, Q.; Zhu, Y.; Shan, J.; et al. *Microchem. J.* **2021**, *169*, No. 106607.

(17) Huang, X.; Di, X.; Zuiderwijk, M. C.; Zhang, L.; Leegwater, H.; Davidse, S.; Kindt, A.; Harms, A.; Hankemeier, T.; Le Dévédec, S. E.; et al. *Talanta* **2024**, *283*, No. 127127.
(18) Zhang, Y.; Liu, Y.; Li, L.; Wei, J.; Xiong, S.; Zhao, Z. *Talanta* **2016**, *150*, 88−96.
(19) Wolrab, D.; Chocholouskova, M.; Jirasko, R.; Peterka, O.; Muzakova, V.; Studentova, H.; Melichar, B.; Holcapek, M. *Anal. Chim. Acta* **2020**, *1137*, 74−84.
(20) Lange, M.; Ni, Z. X.; Criscuolo, A.; Fedorova, M. *Chromatographia* **2019**, *82* (1), 77−100.
(21) Kofeler, H. C.; Ahrends, R.; Baker, E. S.; Ekroos, K.; Han, X.; Hoffmann, N.; Holcapek, M.; Wenk, M. R.; Liebisch, G. *J. Lipid Res.* **2021**, *62*, No. 100138.
(22) Baker, P. R.; Armando, A. M.; Campbell, J. L.; Quehenberger, O.; Dennis, E. A. *J. Lipid Res.* **2014**, *55* (11), 2432−2442.
(23) Xu, T.; Hu, C.; Xuan, Q.; Xu, G. *Anal. Chim. Acta* **2020**, *1137*, 156−169.
(24) Wang, Q.; Ye, M.; Xu, L.; Shi, Z. G. *Anal. Chim. Acta* **2015**, *888*, 182−190.
(25) Pham, T. H.; Zaeem, M.; Fillier, T. A.; Nadeem, M.; Vidal, N. P.; Manful, C.; Cheema, S.; Cheema, M.; Thomas, R. H. *Sci. Rep.* **2019**, *9* (1), 5048.
(26) Vasku, G.; Peltier, C.; He, Z.; Thuret, G.; Gain, P.; Gabrielle, P. H.; Acar, N.; Berdeaux, O. *J. Lipid Res.* **2023**, *64* (3), No. 100343.
(27) Zhou, J.; Liu, H.; Liu, Y.; Liu, J.; Zhao, X.; Yin, Y. *Anal. Chem.* **2016**, *88* (8), 4478−4486.
(28) Peti, A. P. F.; Locachevic, G. A.; Prado, M. K. B.; de Moraes, L. A. B.; Faccioli, L. H. *J. Mass Spectrom.* **2018**, *53* (5), 423−431.
(29) Gao, X.; Lin, L.; Hu, A.; Zhao, H.; Kang, L.; Wang, X.; Yuan, C.; Yang, P.; Shen, H. *Talanta* **2022**, *245*, No. 123475.
(30) Wang, J.; Wang, C.; Han, X. *Anal. Chim. Acta* **2019**, *1061*, 28−41.
(31) Wang, M.; Wang, C.; Han, X. *Mass Spectrom. Rev.* **2017**, *36* (6), 693−714.
(32) Zhou, J.; Yin, Y. *Analyst* **2016**, *141* (23), 6362−6373.
(33) Duranton, F.; Laget, J.; Gayrard, N.; Saulnier-Blache, J. S.; Lundin, U.; Schanstra, J. P.; Mischak, H.; Weinberger, K. M.; Servel, M. F.; Argiles, A. *J. Clin. Lipidol.* **2019**, *13* (1), 176−185.e8.
(34) Hirano, T.; Satoh, N.; Kodera, R.; Hirashima, T.; Suzuki, N.; Aoki, E.; Oshima, T.; Hosoya, M.; Fujita, M.; Hayashi, T.; Ito, Y. *J. Diabetes Investig.* **2022**, *13* (4), 657−667.
(35) Suh, S. H.; Kim, S. W. *Diabetes Metab. J.* **2023**, *47* (5), 612−629.
(36) Mitrofanova, A.; Merscher, S.; Fornoni, A. *Nat. Rev. Nephrol.* **2023**, *19* (10), 629−645.
(37) Kind, T.; Liu, K. H.; Lee, D. Y.; DeFelice, B.; Meissen, J. K.; Fiehn, O. *Nat. Methods* **2013**, *10* (8), 755−758.
(38) Gao, L.; Ji, S.; Burla, B.; Wenk, M. R.; Torta, F.; Cazenave-Gassiot, A. *Anal. Chem.* **2021**, *93* (6), 3163−3171.
(39) Lee, C. H.; Tang, S. C.; Kuo, C. H. *Anal. Chim. Acta* **2021**, *1184*, No. 339014.
(40) Lee, C. H.; Wang, C. Y.; Kao, H. L.; Wu, W. K.; Kuo, C. H. *Anal. Chem.* **2023**, *95* (46), 16902−16910.
(41) Huynh, K.; Barlow, C. K.; Jayawardana, K. S.; Weir, J. M.; Mellett, N. A.; Cinel, M.; Magliano, D. J.; Shaw, J. E.; Drew, B. G.; Meikle, P. J. *Chem. Biol.* **2019**, *26* (1), 71−84.e4.
(42) Okudaira, M.; Inoue, A.; Shuto, A.; Nakanaga, K.; Kano, K.; Makide, K.; Saigusa, D.; Tomioka, Y.; Aoki, J. *J. Lipid Res.* **2014**, *55* (10), 2178−2192.
(43) Sugasini, D.; Subbaiah, P. V. *PLoS One* **2017**, *12* (11), No. e0187826.
(44) Fernandez, R.; Garate, J.; Lage, S.; Teres, S.; Higuera, M.; Bestard-Escalas, J.; Lopez, D. H.; Guardiola-Serrano, F.; Escriba, P. V.; Barcelo-Coblijn, G.; Fernandez, J. A. *J. Am. Soc. Mass Spectrom.* **2016**, *27* (2), 244−254.
(45) FDA. *Bioanalytical Method Validation Guidance for Industry*. https://www.fda.gov/files/drugs/published/Bioanalytical-Method-Validation-Guidance-for-Industry.pdf (accessed Apr 14, 2025).
(46) EMA. *ICH guideline M10 on bioanalytical method validation*. https://www.ema.europa.eu/en/documents/scientific-guideline/draft-ich-guideline-m10-bioanalytical-method-validation-step-2b_en.pdf (accessed Apr 14, 2025).
(47) Carpenter, J. M.; Hynds, H. M.; Bimpeh, K.; Hines, K. M. *ACS Meas. Sci. Au* **2024**, *4* (1), 104−116.
(48) Coradduzza, D.; Azara, E.; Medici, S.; Arru, C.; Solinas, T.; Madonia, M.; Zinellu, A.; Carru, C. *J. Chromatogr. B Analyt. Technol. Biomed. Life Sci.* **2021**, *1162*, No. 122468.
(49) Dai, J.; Lin, H.; Pan, Y.; Sun, Y.; Wang, Y.; Qiao, J. Q.; Lian, H. Z.; Xu, C. X. *Food Chem.* **2023**, *403*, No. 134298.
(50) Adams, K. J.; Pratt, B.; Bose, N.; Dubois, L. G.; St John-Williams, L.; Perrott, K. M.; Ky, K.; Kapahi, P.; Sharma, V.; MacCoss, M. J.; Moseley, M. A.; Colton, C. A.; MacLean, B. X.; Schilling, B.; Thompson, J. W.; Alzheimer's Disease Metabolomics Consortium. *J. Proteome Res.* **2020**, *19* (4), 1447−1458.
(51) Jaber, M. A.; de Falco, B.; Abdelrazig, S.; Ortori, C. A.; Barrett, D. A.; Kim, D. H. *Anal. Methods* **2023**, *15* (24), 2925−2934.
(52) Mandal, R.; Zheng, J.; Zhang, L.; Oler, E.; LeVatte, M. A.; Berjanskii, M.; Lipfert, M.; Han, J.; Borchers, C. H.; Wishart, D. S. *Anal. Chem.* **2025**, *97* (1), 667−675.
(53) Cai, Y.; Chen, X.; Ren, F.; Wang, H.; Yin, Y.; Zhu, Z. J. *Analyst* **2024**, *149* (20), 5063−5072.
(54) Wei, F.; Lamichhane, S.; Orešič, M.; Hyötyläinen, T. *TrAC, Trends Anal. Chem.* **2019**, *120*, No. 115664.
(55) Cebo, M.; Fu, X.; Gawaz, M.; Chatterjee, M.; Lammerhofer, M. *J. Pharm. Biomed. Anal.* **2020**, *189*, No. 113426.
(56) Cajka, T.; Smilowitz, J. T.; Fiehn, O. *Anal. Chem.* **2017**, *89* (22), 12360−12368.
(57) Miyamoto, Y.; Miyazaki, T.; Honda, A.; Shimohata, H.; Hirayama, K.; Kobayashi, M. *J. Clin. Biochem. Nutr.* **2016**, *59* (3), 199−206.
(58) Kaysen, G. A. *Kidney Int.* **2006**, *70*, S55−S58.
(59) Haas, M.; Kerjaschki, D.; Mayer, G. *Kidney Int. Suppl.* **1999**, *71*, S110−S112.
(60) Graessler, J.; Schwudke, D.; Schwarz, P. E.; Herzog, R.; Shevchenko, A.; Bornstein, S. R. *PLoS One* **2009**, *4* (7), No. e6261.
(61) Lee, M.; Lee, S. Y.; Bae, Y. S. *Exp. Mol. Med.* **2023**, *55* (6), 1110−1130.
(62) Dong, L.; Tan, J.; Zhong, Z.; Tang, Y.; Qin, W. *Clin. Chim. Acta* **2023**, *549*, No. 117561.
(63) Jimenez-Rojo, N.; Leonetti, M. D.; Zoni, V.; Colom, A.; Feng, S.; Iyengar, N. R.; Matile, S.; Roux, A.; Vanni, S.; Weissman, J. S.; Riezman, H. *Curr. Biol.* **2020**, *30* (19), 3775−3787.e7.
(64) Mandrekar, J. N. *J. Thorac. Oncol.* **2010**, *5* (9), 1315−1316.
(65) Quell, J. D.; Romisch-Margl, W.; Haid, M.; Krumsiek, J.; Skurk, T.; Halama, A.; Stephan, N.; Adamski, J.; Hauner, H.; Mook-Kanamori, D.; Mohney, R. P.; Daniel, H.; Suhre, K.; Kastenmüller, G. *Metabolites* **2019**, *9* (6), 109.
(66) Brown, E. M.; Clardy, J.; Xavier, R. J. *Cell Host Microbe* **2023**, *31* (2), 173−186.
(67) Jenkins, B. J.; et al. *Biosynthesis and Glucose Intolerance. Sci. Rep.* **2017**, *7*, 44845.
(68) Lv, W.; Zeng, Z.; Zhang, Y.; Wang, Q.; Wang, L.; Zhang, Z.; Shi, X.; Zhao, X.; Xu, G. *Anal. Chim. Acta* **2022**, *1215*, No. 339979.
(69) Li, P.; Lammerhofer, M. *Anal. Chem.* **2021**, *93* (27), 9583−9592.
(70) Wang, S.; Li, J.; Shi, X.; Qiao, L.; Lu, X.; Xu, G. *J. Chromatogr. A* **2013**, *1321*, 65−72.
(71) Pirok, B. W. J.; Stoll, D. R.; Schoenmakers, P. J. *Anal. Chem.* **2019**, *91* (1), 240−263.
(72) Sorensen, M. J.; Miller, K. E.; Jorgenson, J. W.; Kennedy, R. T. *J. Chromatogr. A* **2023**, *1687*, No. 463707.

https://doi.org/10.1021/acs.analchem.4c06409
Anal. Chem. 2025, 97, 9713−9721